From co-crystals to functional thin films: photolithography using the [2+2] photodimerization

Suman Ghorai,[a,b] Joseph C. Sumrak,[a,b] Kristin M. Hutchins,[a] Dejan-Krešimir Bučar,[a] Alexei V. Tivanski,[a,]* and Leonard R. MacGillivray[a,]*

[a] Department of Chemistry, University of Iowa, Iowa City, IA, 52242 USA.

[b] Authors contributed equally to work.

E-mail: alexei-tivanski@uiowa.edu; len-macgillivray@uiowa.edu

Contents

1) Experimental Information

AFM Measurements. AFM imaging was conducted using a molecular force probe 3D AFM (Asylum Research, Santa Barbara, CA). Height images were collected at room temperature using silicon probes (MikroMasch, San Jose, CA, CSC37) with a nominal spring constant of 0.35 Nm^{-1} and a typical tip radius of curvature of 10 nm.

STXM Measurements. STXM measurements were performed on samples deposited on Si_3N_4 windows (Silson Ltd., England) with similar spin coating conditions. Single energy images and oxygen (O) K-edge Near Edge X-ray Absorption Fine Structure (NEXAFS) spectra were acquired using STXM instrument on Beamline 5.3.2 of the Advanced Light Source at Lawrence Berkeley National Laboratory (Berkeley, CA). For STXM measurements, the X-ray beam is focused with a custom made Fresnel zone plate onto the sample, and the transmitted light intensity is detected. The diffraction limited spot size at the sample was ~25 nm. Images at a single energy were obtained by raster-scanning the sample at the focal plane of X-rays and collecting transmitted monochromatic light as a function of sample position. Spectra at each image pixel or a particular sample region are extracted from a collection of images recorded at multiple photon energies across the absorption edge. Dwell times used to acquire an image at single photon energy were typically 0.5 ms per pixel.

Single-crystal X-ray data. All crystal data were measured on a Nonius Kappa CCD single-crystal X-ray diffractometer at room temperature using MoKα radiation (λ = 0.7107 Å). After anisotropic refinement of non-hydrogen atoms, H-atoms bonded to sp^2 hybridized atoms were placed in idealized positions and allowed to ride on the atom to which they are attached. The hex-phgl H-atoms were calculated in an optimal hydrogen-bonding geometry. Structure solution was accomplished with the aid of SHELXS-97 and refinement was conducted using SHELXL-97. Crystal data for 2(hex-phgl)·2(4,4'-bpe)·2(1,3-dichlorobenzene): triclinic, P ī, a = 8.367(1) Å, b = 10.824(1) Å, c = 17.212(2) Å, α = 84.43(1), β = 79.71(1)°, γ = 75.29(1), V = 1481.1(3) Å3, D_c = 1.272 g cm^{-3}, Z = 2, F(000) = 596, μ = 0.257 mm^{-1}, MoK_α radiation (λ = 0.71070 Å), T = 298(2) K, and R = 0.086 for 2679 reflections with $I_{net} > 2\sigma(I)$ (CCDC-926350).

2) Solubility tests

Table S1. Solubility data for thin films based on 4,4'-bpe and hex-phgl.

Solvent	Concentration (mg/ml)	Spin coating speed (rpm)	Comment*
EtOH	6	300	1
	6	500	1
	6	1000	1
	12	500	1
	12	1000	1
EtOH +Diethyl Ether	12	1000	1
	12	1500	1
IPA	12	slow evaporated	2
	12	100	3
	12	200	3
	12	300	3
	12	500	3
	12	1000	3
	12	1500	3
	6	1000	3
CH_3CN	12	1000	1
	6	1000	1
	6	1000	1
	6	1000	1
1:1 IPA:di-Cl Benzene	6	300	4
	6	500	4
	6	1000	5
	12	300	4
	12	500	4
	12	1000	4
	9	500	5
	9	1000	6

**1: single crystal; 2: non-continuous film-like morphology; 3: layered structure; 4: film with relatively high roughness (greater than 60 nm); 5: film with lower roughness (lower than 35nm); 6: smooth film (15-20 nm roughness).*

Solubility tests performed to determine a solvent that produces a uniform thin film. Concentrations and spin coating rates also varied to determine conditions for film formation.

3) AFM images of trials with different solvents, template, and spin coating conditions

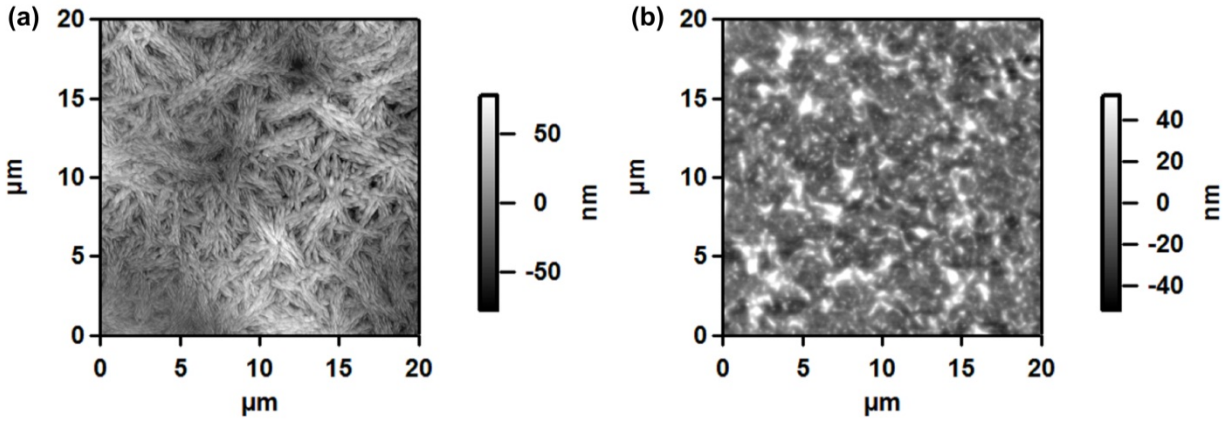

Figure S1. Morphology of thin film trials with (a) hex-phgl and 4,4'-bpe dissolved in IPA at 12 mg/ml with a spin coating speed of 1000 rpm and (b) hex-phgl and 4,4'-bpe dissolved in 1:1 mixture of 1,3-dichlorobenzene and IPA and the morphology is obtained by slow evaporation. Images show the morphology of the thin film trials using hex-phgl template at different solvents. We optimized the solvent and spin coating conditions to improve the morphology of the thin film (Fig. S1a,b).

4) IR Spectroscopy

IR spectroscopy performed using a Nicolet 380 FT-IR Spectrometer. The KBr press method was used for single components hex-phgl and 4,4'-bpe, as well as the co-crystal. An IR spectrum of the thin film was collected using an ATIR.

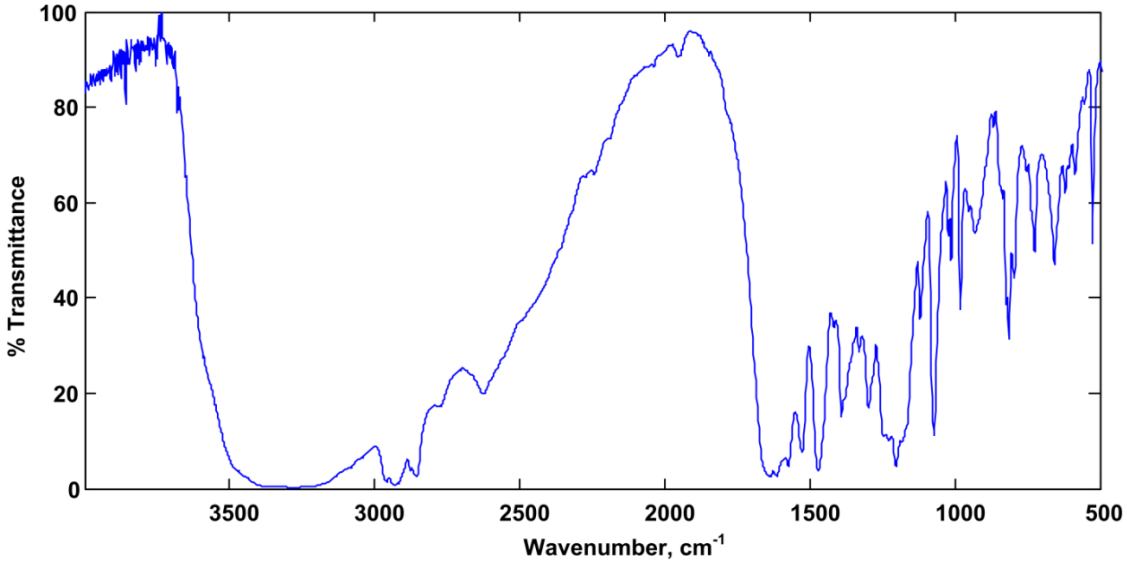

Figure S2. IR spectrum of hex-phgl.

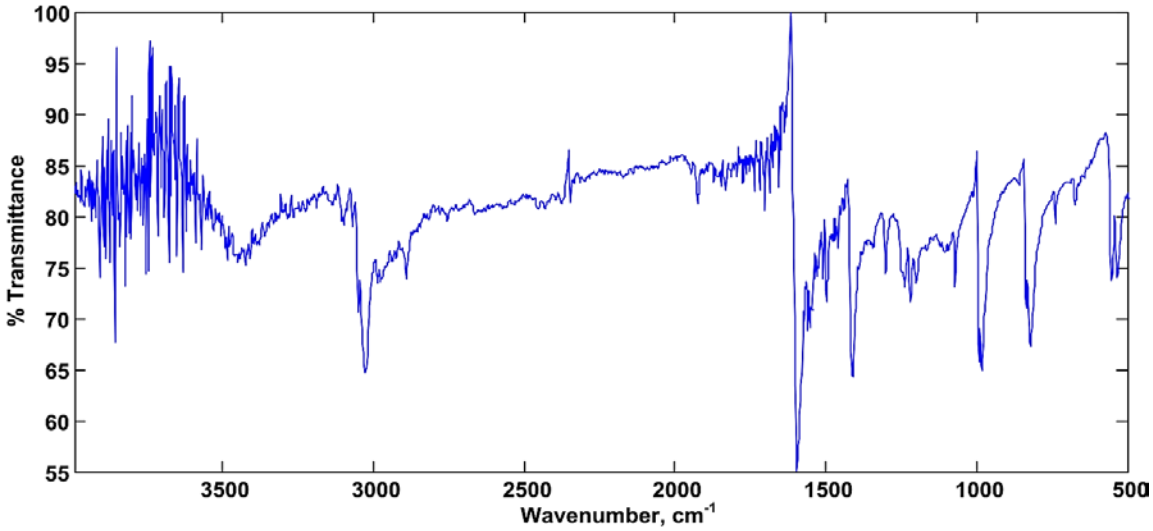

Figure S3. IR spectrum of 4,4'-bpe.

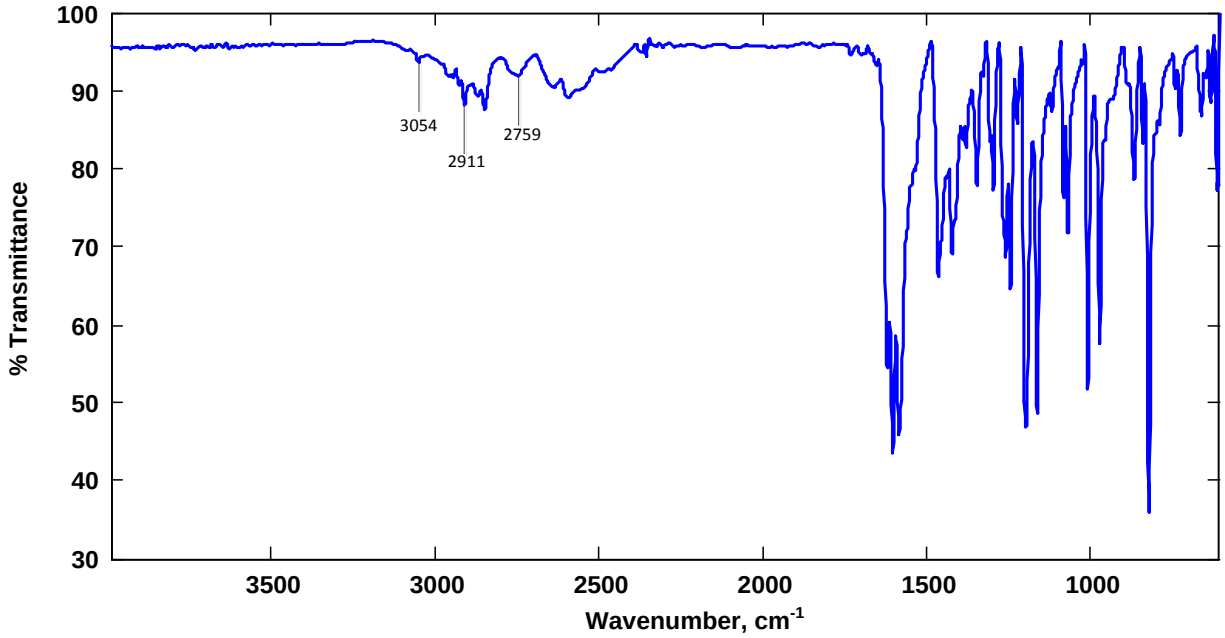

Figure S4. IR spectrum of (4,4'-bpe)·(hex-phgl). Labeled peaks correspond to (phenol)O-H···N(pyridine) forces.

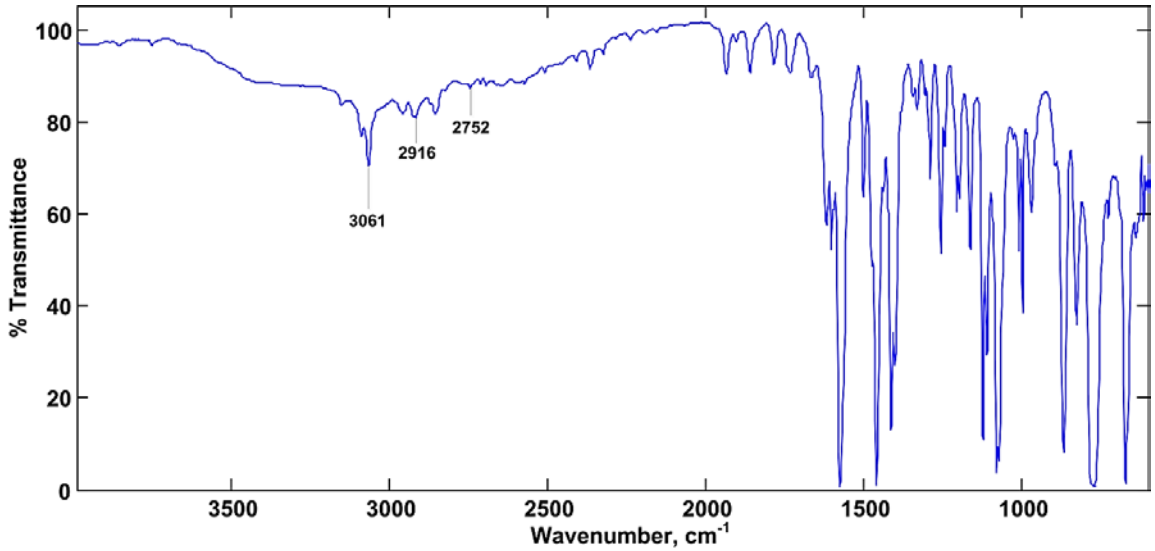

Figure S5. IR spectrum of 4,4'-bpe and hex-phgl thin film. Labeled peaks correspond to (phenol)O-H···N(pyridine) forces.

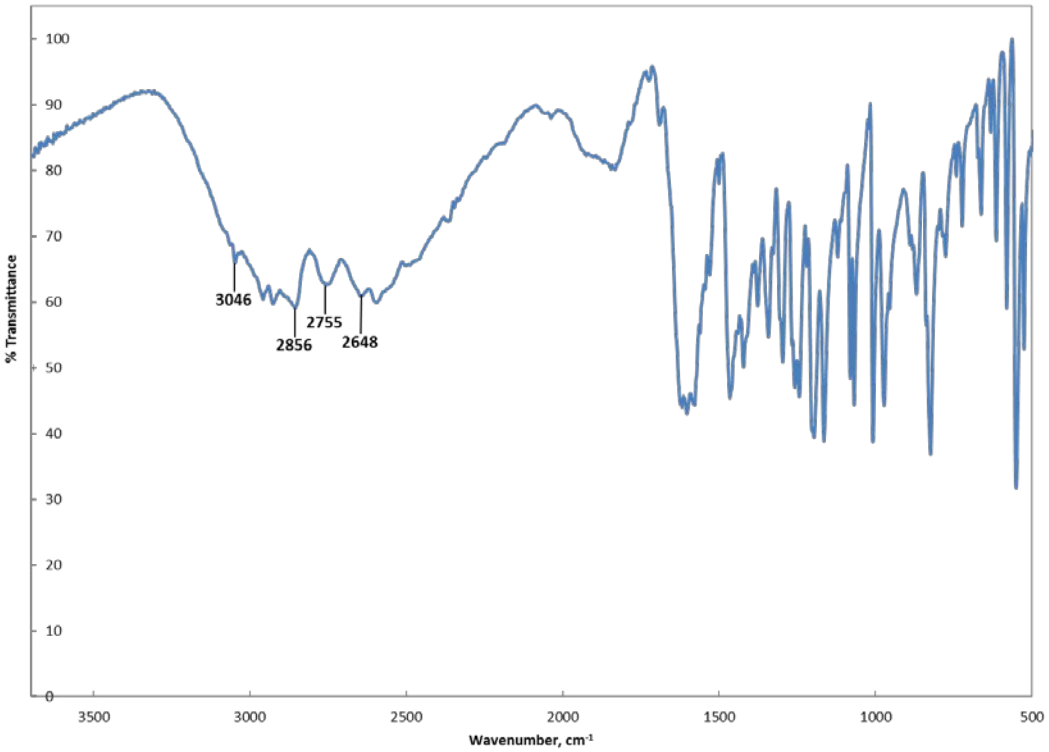

Figure S6. IR spectrum of 4,4'-bpe and hex-phgl prepared *via* solvent evaporation. Labeled peaks correspond to (phenol)O-H···N(pyridine) forces.

5) Powder X-ray diffraction data

PXRD data were collected from samples mounted on glass slides using a Siemens D5000 X-ray diffractometer using $CuK_{\alpha 1}$ radiation (λ = 1.54056 Å) (scan type: locked coupled; scan mode: continuous; step size: 0.02°).

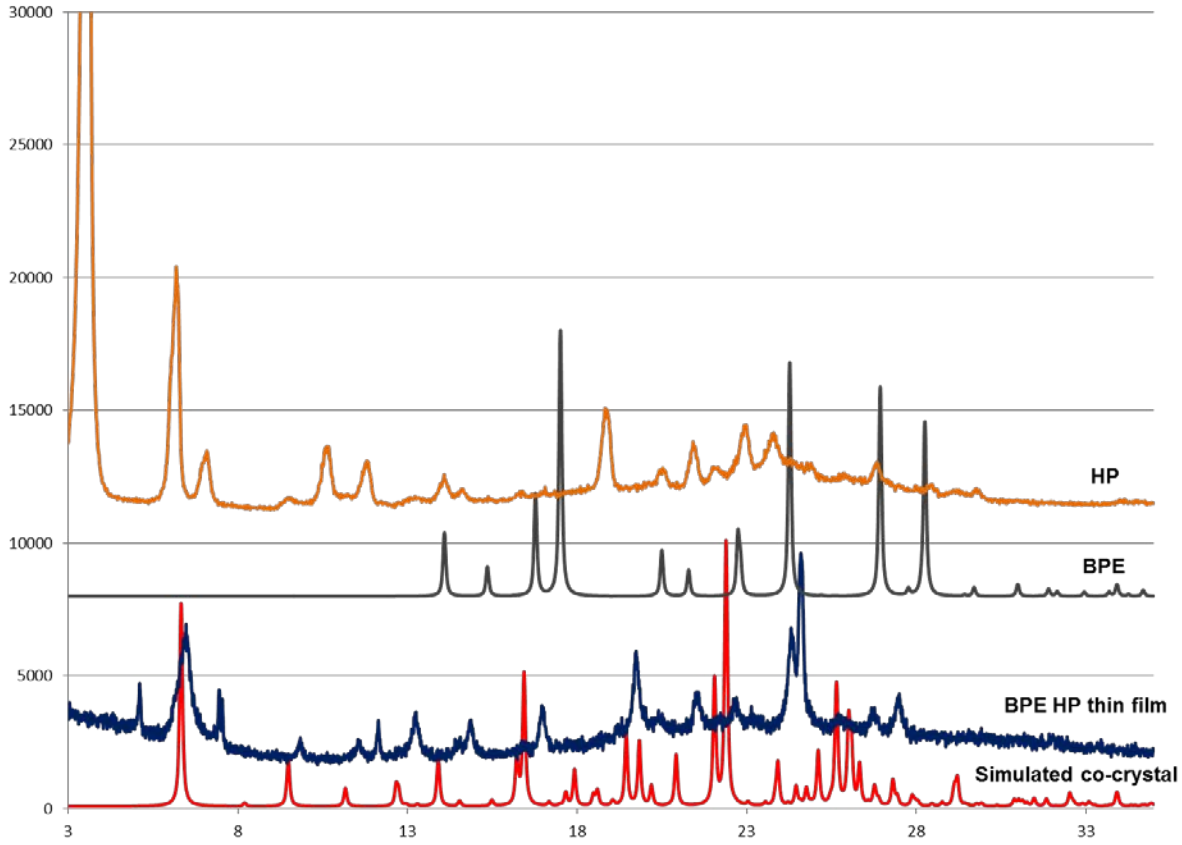

Figure S7. Comparison of powder pattern of the thin film, co-crystal, and individual components (HP = hex-phgl; BPE = 4,4'-bpe).

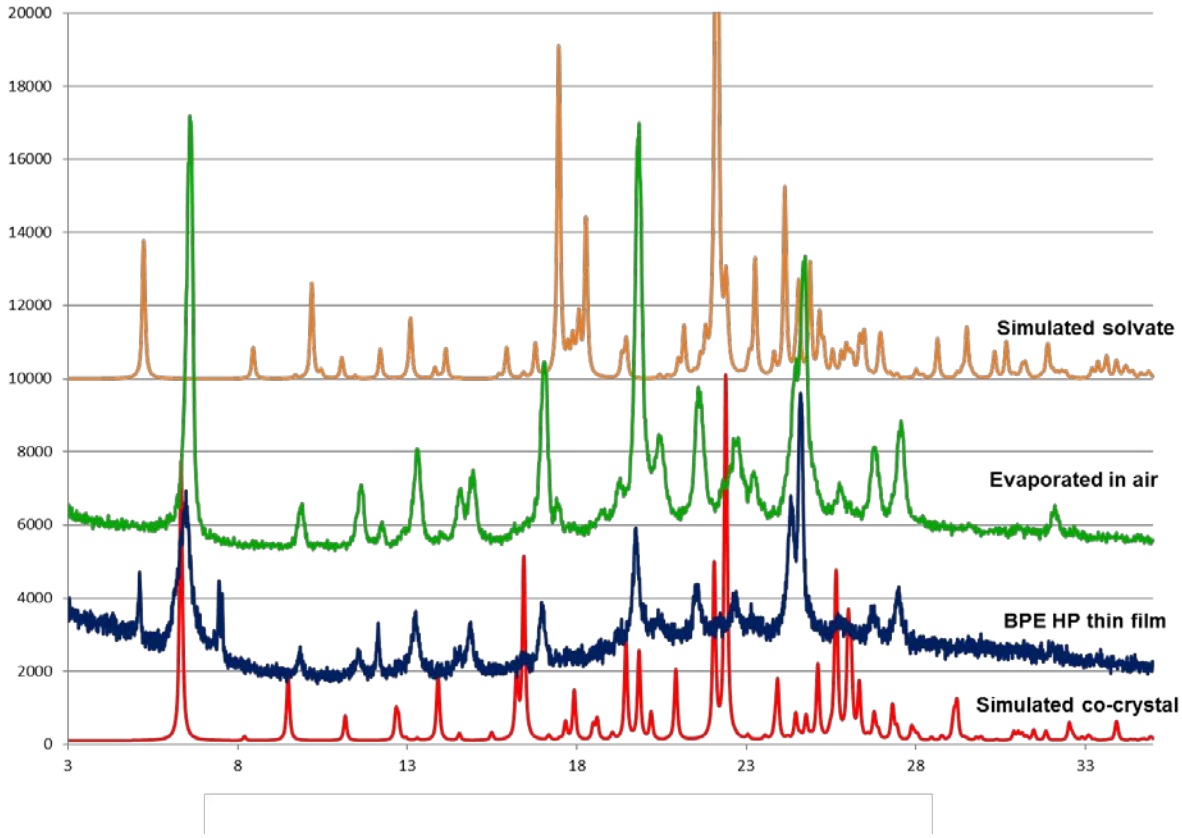

Figure S8. Comparisons of PXRD powder patterns of solvated co-crystal (gold), co-crystal evaporated to dryness (green), as prepared thin film (dark blue), and reported non-solvated co-crystal (red). Additional peaks are attributed to pure components and/or other phases associated with the co-crystallization.

6) Dissolution rate measurement on the thin film

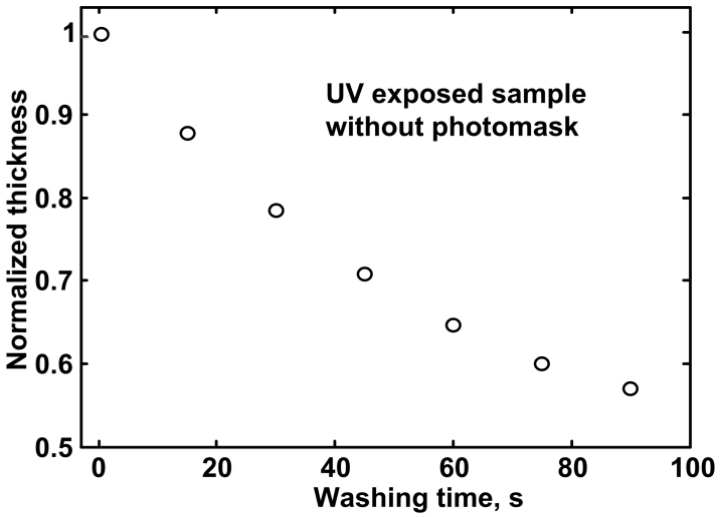

Figure S9. Graph showing changes in thickness of the photoreacted thin film normalized to the initial thickness plotted as a function of washing time in a mixture of pentane and ether (2:1 *v*/*v*).

Solubility differences between the unreacted and photoreacted thin film utilized to develop the photo patterns on the thin film. After 90 sec of washing, more than half of the photoreacted film thickness remained, whereas the unreacted film dissolved within approximately 2 s of washing in the same solvent system.

7) ESI Mass Spectrometry

ESI mass spectrometry performed using a Waters Q-Tof Premier Mass Spectrometer.

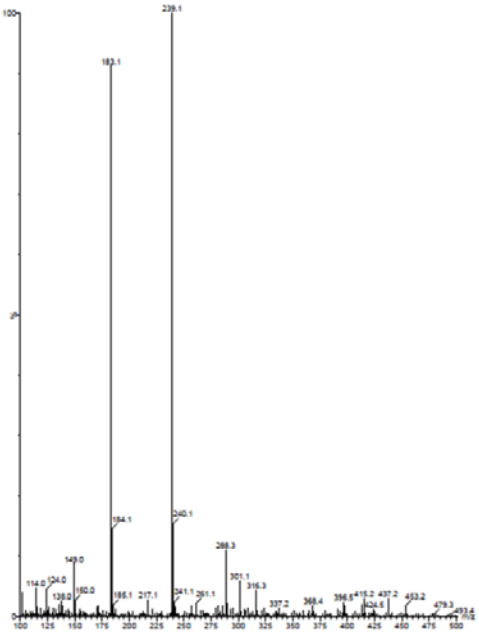

Figure S10. ESI mass spectrum films containing 4,4´-bpe and hex-phgl before UV exposure.

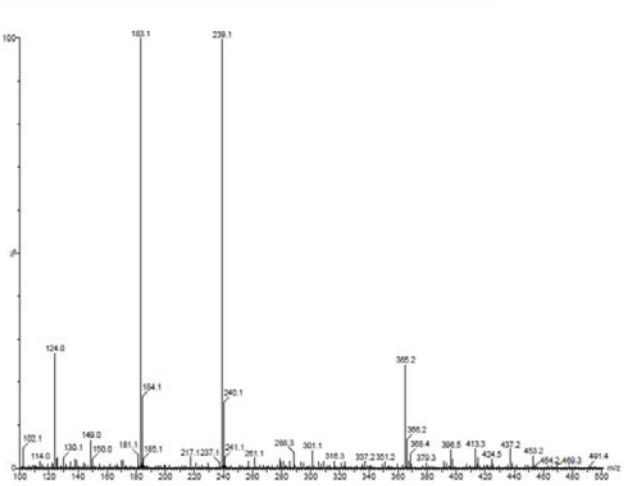

Figure S11. ESI mass spectrum films of 4,4´-bpe and hex-phgl after 20 h UV exposure.

Mass spectrometry performed on samples of four unreacted thin films and four reacted films. Samples were dissolved in methanol to form a stock solution. From the solution, 30 μL was diluted with a 1:1 water: acetonitrile with an additional 0.1 % formic acid solution. The peak at 183 au of the unreacted thin film is consistent with monoprotonated 4,4'-bpe. The peak at 239

au is consistent with monoprotonated hex-phgl. Upon irradiation, a peak at 365 au appears in the spectrum, consistent with monoprotonated 4,4’ tpcb. Base peak after reaction at 183 au is likely due to unreacted 4,4’-bpe and/or diprotonated tpcb, which have equal mass to charge ratios.

8) ^{1}H NMR Spectroscopy

^{1}H NMR data collected on an AVANCE Bruker NMR spectrometer operating at 300 or 400 MHz using DMSO-d_6 as the solvent.

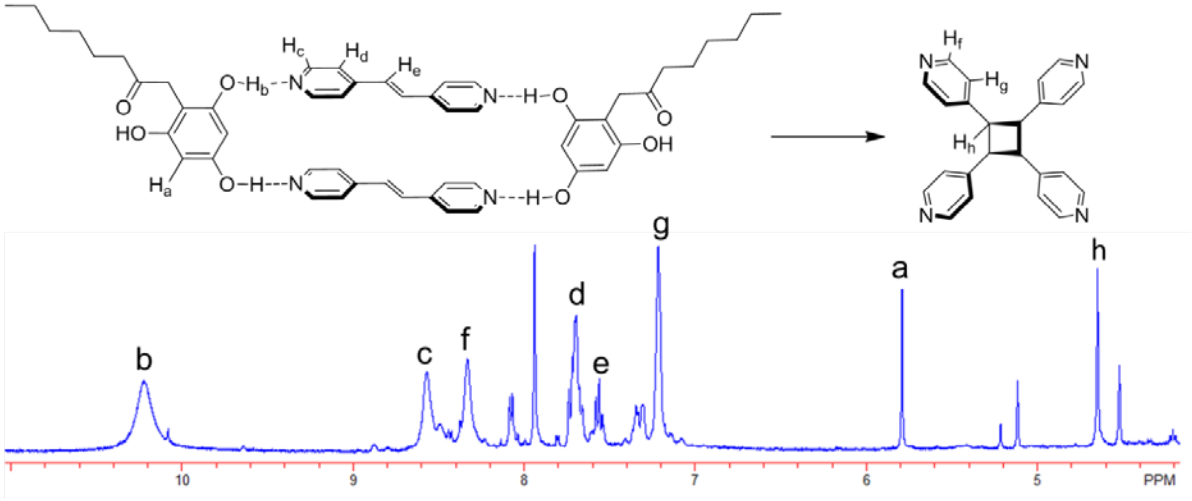

Figure S12. ^{1}H-NMR spectrum of (4,4'-bpe)·(hex-phgl) after UV irradiation. (400 MHz)

To collect a ^{1}H NMR spectrum, 80 thin films were exposed to UV irradiation for 20 h. The reacted thin films were concentrated into a single sample by dissolving each thin film in ethanol and combing the samples. The peaks at 8.6 and 8.3 ppm are assigned to the α-hydrogens of the pyridine rings. The ratio of the peaks to the cyclobutane peak demonstrates approximately a 50% photoreaction in the thin films.

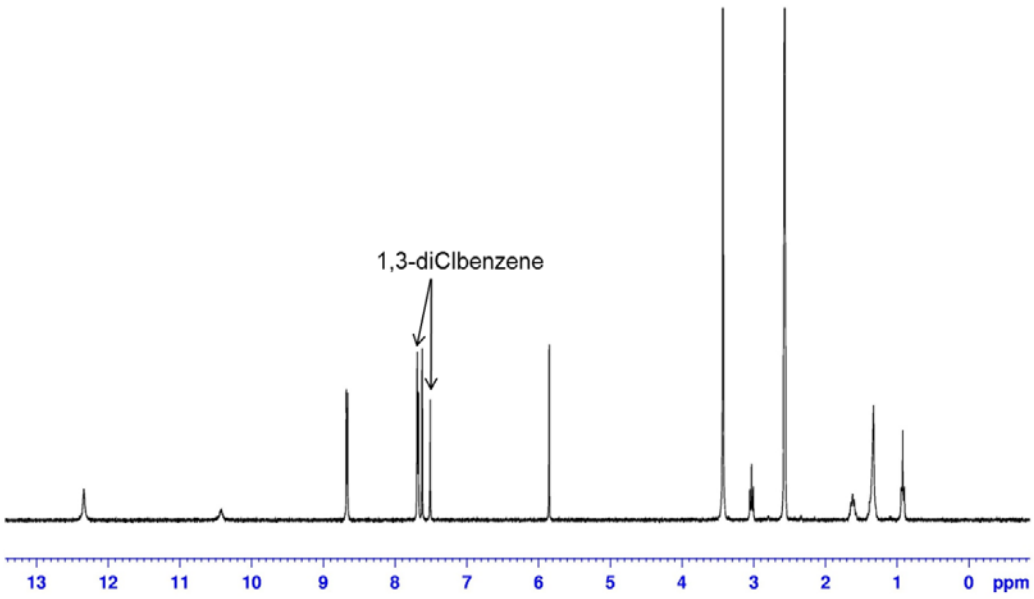

Figure S13. ^{1}H-NMR spectrum of solvated (4,4'-bpe)·(hex-phgl) co-crystal.

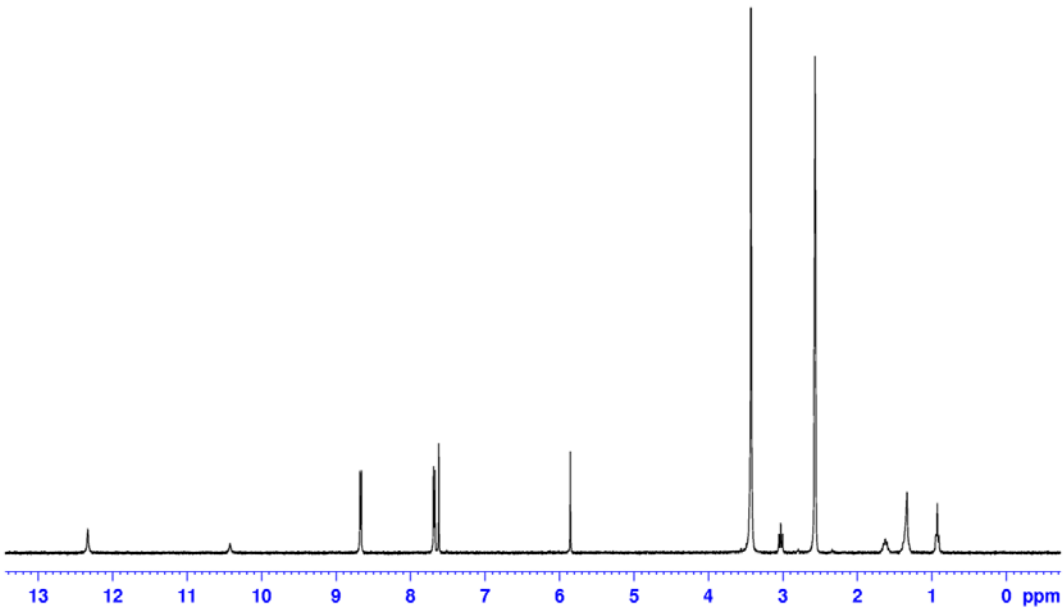

Figure S14. ^{1}H-NMR spectrum of (4,4'-bpe)·(hex-phgl) co-crystal after evaporation to dryness. Note the lack of 1,3-dichlorobenzene being present in the sample.

9) Thermogravimetric Analysis

TGA data were collected on an EXSTAR 6000 TG/DTA.

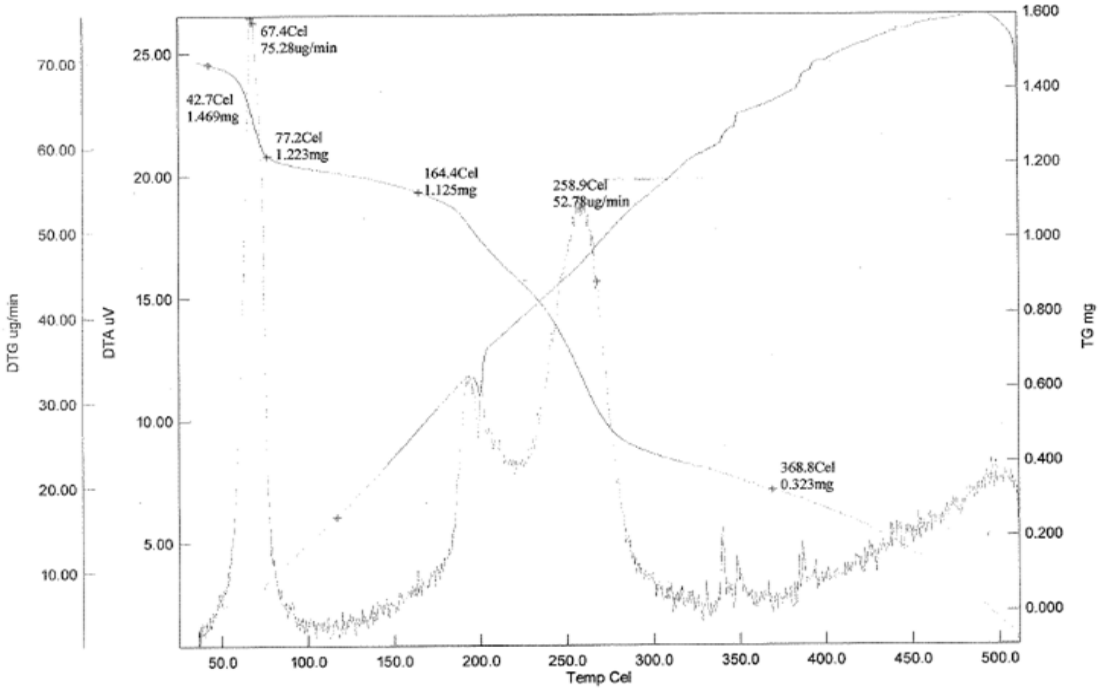

Figure S15. TGA of solvated co-crystal showing loss of 1,3-dichlorobenzene that occurs slightly above room temperature.

10) STXM images

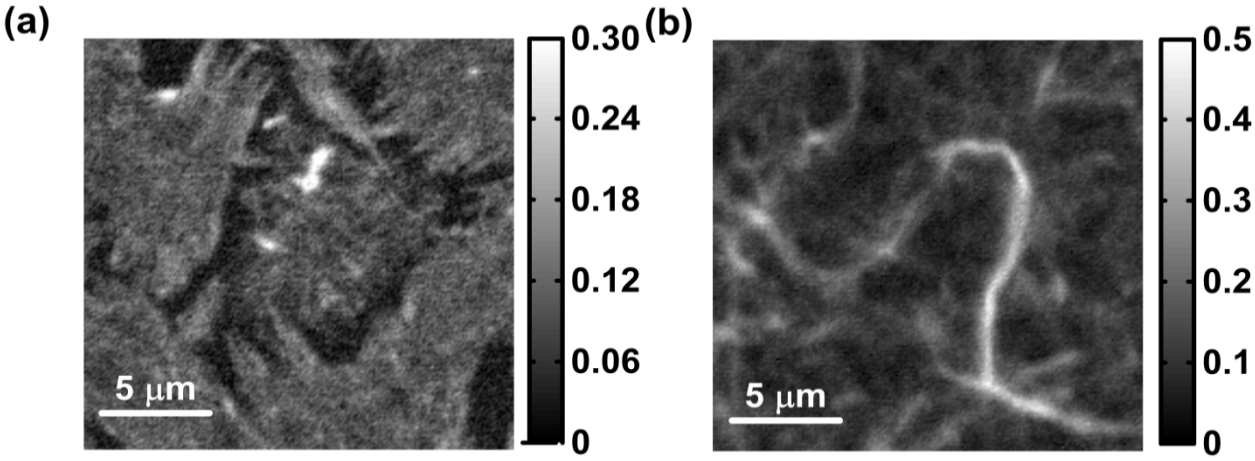

Figure S16. STXM images of thin films prepared on a Si_3N_4 membrane. The NEXAFS spectra were collected on the same region of this thin film.

11) NEXAFS spectral data

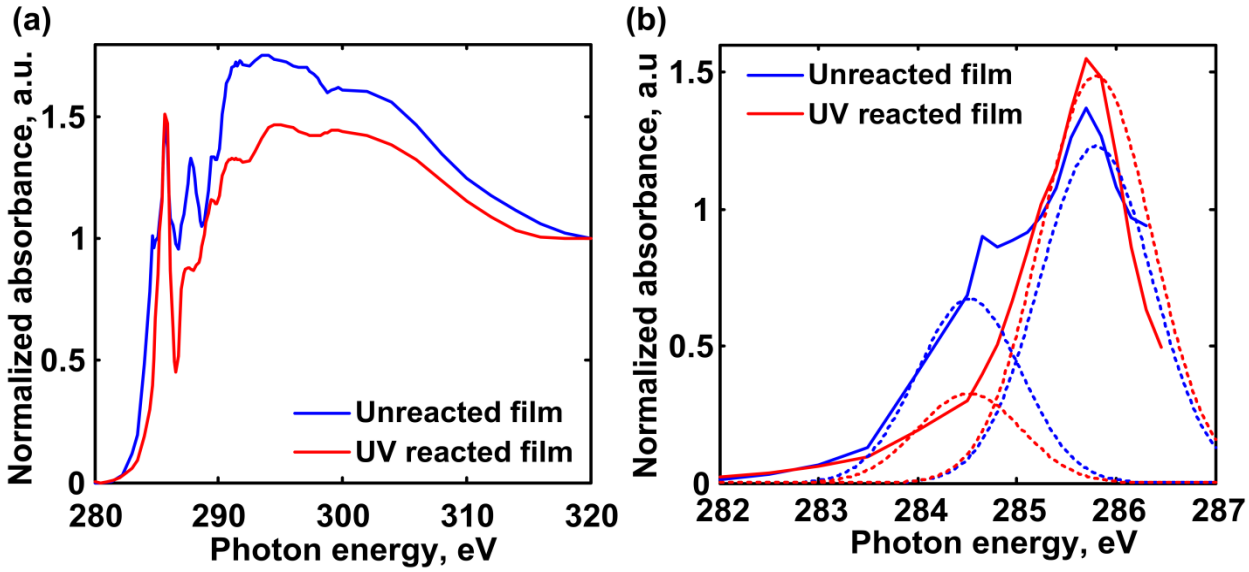

Figure S17. (a) C K-edge NEXAFS spectra of the thin film prepared on Si_3N_4 window using the same conditions. (b) Narrower energy range of the C K-edge spectra showing two different transitions for aromatic and nonaromatic C=C at 285.8 and 284.6 eV, respectively. The combined Gaussians fit of the spectra was used to calculate the extent of reaction, *ca* 50%, which is consistent with the result obtained using NMR.

Table S2. Gaussian fit parameters for thin film NEXAFS spectra (Fig. S17b).

Gaussian Peaks	***Parameters***	***Unreacted thin film***	***Reacted thin film***
Peak 1: Non aromatic C=C	Normalized absorption	0.6718	0.3262
	Peak center, eV	284.52	284.52
	Width, eV	0.5226	0.5226
Peak 2: Aromatic C=C	Normalized absorption	1.23	1.4854
	Peak center, eV	285.8	285.8
	Width, eV	0.5662	0.5662

Lower energy peak at 284.6 eV is resonance transition in the NEXAFS spectra due to non-aromatic C=C; whereas the higher energy peak at 285.8 eV occurs due to the aromatic C=C functional group. The absorbance for these two transitions needs to be separated in order to quantify the extent of photodimerization reaction accurately. Initially, unreacted film NEXAFS spectrum was fit by a sum of two Gaussian functions that correspond to transitions for aromatic and non-aromatic C=C, yielding peak width and peak center for each transition. Then, obtained peak center and width were fixed for the fit of reacted thin film with only normalized absorbance for both transitions used as free fit parameter. Table S2 lists parameters obtained from the fit for both unreacted and reacted thin films. The extent of photoreaction can then be obtained by determining the ratio of normalized absorbance of the non-aromatic C=C at 284.6 eV for reacted

and unreacted films. The value for extent of reaction was ~ 50% using this method, consistent with the NMR data.

12) AFM images and height profiles thin films of 4,4'-bpe and hex-phgl.

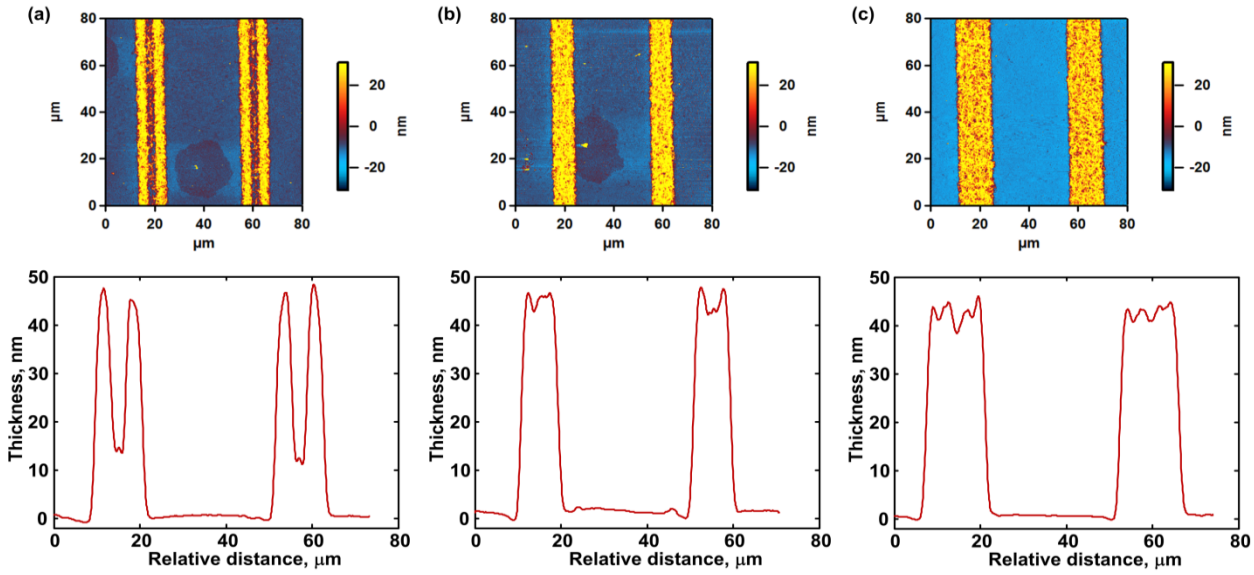

Figure S18. AFM images of UV exposed thin film with photomask of 4,4'-bpe and hex-phgl, followed by washing with the solvent. The sharp features were the reacted portion of the thin film which was uncovered by the photomask while UV exposure. Obtained features were consistent with the type of photomask used.